

# **Experimental and numerical study on structural behavior of a single timber Textile Module**

M. Sistaninia, M. Hudert, L. Humbert\*, Y. Weinand

*IBOIS Laboratory for timber construction, Ecole Polytechnique Fédérale de*

*Lausanne (EPFL), CH-1015 Lausanne, Switzerland*

E-mail: *masoud.sistaninia@epfl.ch, markus.hudert@epfl.ch,*

*laurent.humbert@epfl.ch, yves.weinand@epfl.ch*

\* Corresponding author. Tel.: +41 216 932398; fax: +41 216 932394.

## **Abstract**

The present work investigates an innovative class of timber structure with potential applications in roofing, facade and bridge construction, called Timberfabric. The development of Timberfabric structures originates from the approach of harnessing the structural, modular and aesthetic qualities of textiles in timber construction (Weinand and Hudert, 2010). Timberfabric structures are made of several structural unit cells called Textile Modules. When properly designed, one obtains a modular and lightweight structure with particular geometrical and structural qualities.

This paper focuses on the single timber Textile Module. Based on finite element (FE) method, a reliable procedure is proposed for modeling the overall assembly process of the Textile Module. For comparison, Textile Module prototypes are constructed at two different scales (large and intermediate scales) with different

assembly conditions. The proposed geometrically nonlinear FE model allows evaluating the stresses that are induced during the construction process and may affect the structural integrity of the module. In particular, the risk of failure is identified using the anisotropic Tsai-Hill criterion.

The structural behavior of the timber Textile Module is then investigated through bending tests using the constructed prototypes. During the loading procedure, the vertical deflections are measured at different locations on the prototype surface by means of external displacement transducers. Using the FE model, the corresponding deformed shapes are simulated by applying the bending loads on the pre-stressed Textile Module. Experimental displacements and FE predictions are thus compared and found to be in good agreement.

**Keywords:** Timber Textile Module, Construction stresses, Experimental method, Finite Element modeling.

## **1. Introduction**

Wood is a versatile construction material that is abundant in large parts of the world. Moreover, this is a renewable resource that can be processed and assembled in energy efficient ways. These qualities can be considered as an advantage over other construction materials such as concrete or steel, particularly with regard to globally increasing energy consumption and simultaneously decreasing resources. This, in turn, should increase the interest of the research community in expanding the range of applications of timber structures.

Examples of well-recognized timber architectural forms include among others folded plate structures [1, 2] and lattice structures (e.g. timber lattice roof for the

Mannheim Bundesgartenschau) [2, 3]. They clearly present advantages over more traditional flat-surfaced roofing structures of increasing the efficiency of the structure, reducing its weight and enforcing load carrying capacity.

Recently, a new type of timber structures, called Timberfabric, with particular structural properties has been developed at IBOIS [4, 5]. Its development has been driven by the aim of incorporating textile qualities such as modularity and the mutual support of textile fabrics' constituent elements in timber construction. Timberfabric structures have a high potential for architectural applications due to their versatility, adaptability and their aesthetic qualities, which are directly linked to their structural make-up. They are based on a structural unit cell, the Textile Module, which is depicted in Fig. 1a, and which results from bringing together textile assembly principles with timber components. The double-layered Timberfabric structure shown in Fig. 1b represents only one of many possible configurations of Textile Modules.

a



b

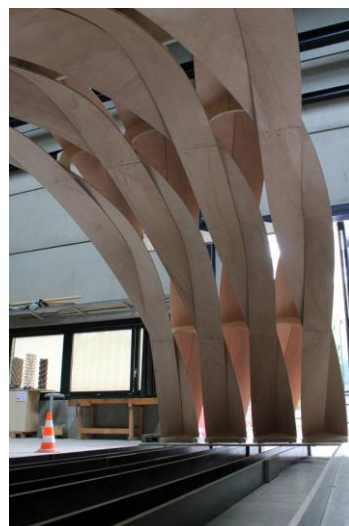


**Fig. 1** (a) Single Textile Module (b) Double-layered Timberfabric structure

The single Textile Module presented in Fig. 1a provides a structural shape of particular interest for this study. Briefly, it consists of two mutually supporting thin panels that become doubly curved during the assembly process as illustrated in Fig. 2. Consequently, construction (or residual) stresses are generated during the fabrication of the module and their amplitude typically depends on the constitutive material, the size of panels as well as the assembly conditions. A poor quality of material as well as inappropriate panel width and thickness may even cause its premature failure during the assembly process. The construction stresses can be evaluated by means of a finite element (FE) model that takes into account the different fabrication stages (Fig. 2).

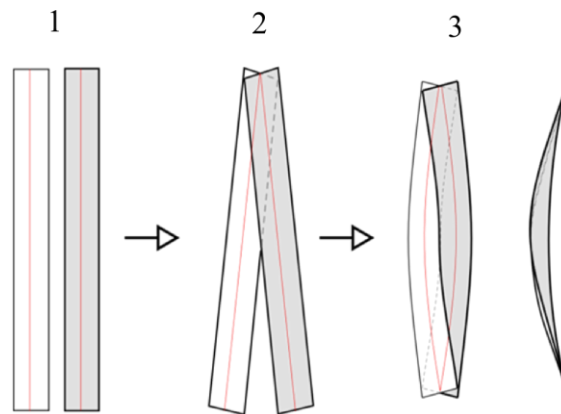


**Fig. 2** Design principle for the Textile Module

This paper focuses on the fabrication process and structural behavior of a representative single Textile Module in a bending load configuration. The proposed approach is both experimental and numerical. It involves the fabrication of two prototypes at two different scales (intermediate and large scale) with different assembly conditions, as discussed in the first part of section 2. The second part of the section is devoted to the bending test setup and required measurement equipment.

Despite of the numerous finite element (FE) models available for braided textile composites [6-10], the numerical study of the timber Textile Module requires special attention as the analysis is complicated by the particular geometry and

assembly conditions encountered. Because of the large deflections and rotations undergone by the module during the fabrication stages (Fig. 2), a geometrically non-linear FE model that aims to accurately reproduce the geometrical shape of the Textile Module is developed in section 3. It is anticipated that this model may permit a representative evaluation of the construction stresses. In section 4, vertical displacements measured at several locations of the prototype surface during the bending tests are compared to the finite element predictions. The structural behavior of the Textile Module is finally discussed.

## 2. Experimental investigations

### 2.1. Materials and specimens

For this study, two textile modules have been constructed: the first one is formed of two GFP laminated wood panels of length  $l = 12.375$  m and width  $w = 0.825$  m while TeboPly™ Okoumé plywood panels of size  $l \times w = 2.34 \times 0.24$  m<sup>2</sup> are used for the second. GFP and Okoumé panels are supplied by Schilliger Holz AG (Switzerland) and Thebault (France) companies, respectively. As illustrated in Fig 3, they consist of three-ply [0/90/0] and four-ply [0/90]<sub>s</sub> symmetric orthotropic laminates, corresponding to respective thicknesses ( $t$ ) of 33 mm and 6.3 mm. As customary, plywood is produced from rotary cut veneers that are bonded with an adhesive (synthetic) resin under high pressure conditions. In each case, the uppermost (face) and lowermost (back) veneers are of equal thickness with the same grain direction along the longitudinal axis ( $L$ -axis) of the laminate. As shown in Fig 3(a) for the three-ply configuration, the symmetry plane passes through the center of the core ply of 13 mm thick and its grain is directed along the transversal axis ( $T$ -axis) of the laminate. For the four-ply layup, the two core plies are of the same thickness (2 mm)

and glued to each other so that their grain direction remain perpendicular to the longitudinal axes of the face veneers (along the  $T$ -axis). This glued interface corresponds to the symmetry plane (middle surface) of the plywood. Such an even-layered arrangement has proven to increase efficiency in veneer manufacturing and grading (less variability) although it adds to the cost of production.

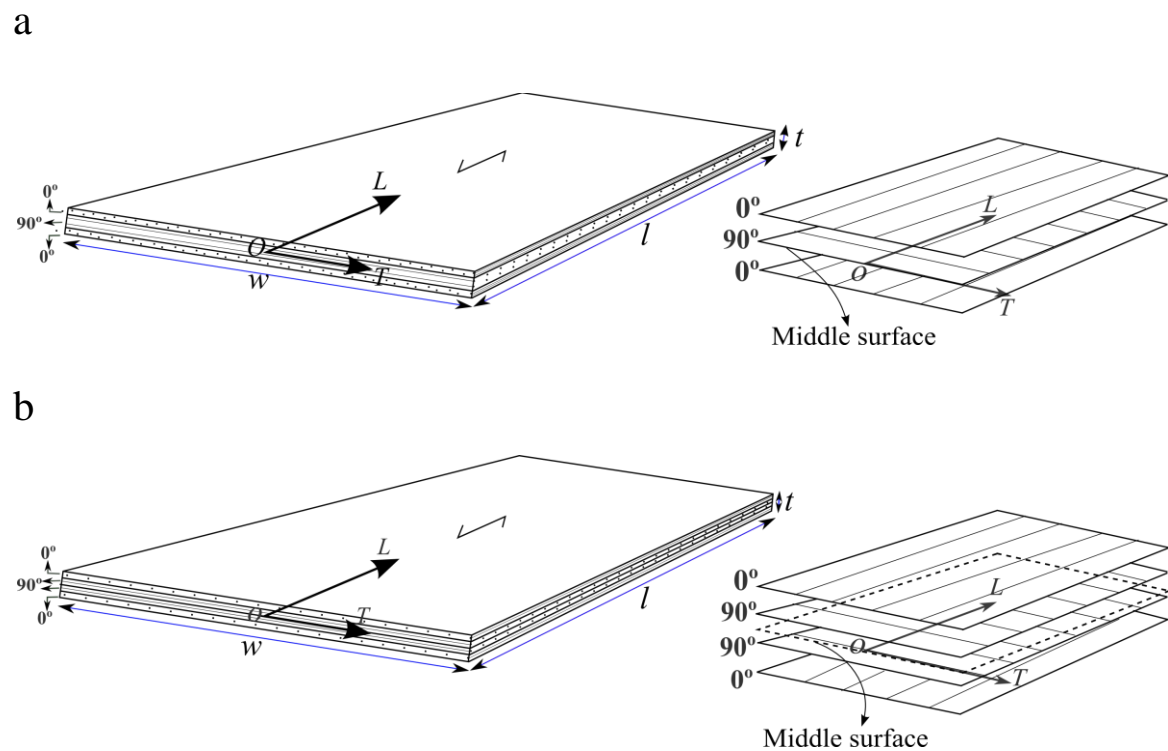


**Fig. 3** (a) GFP and (b) Okoumé plywood layups and local coordinate system ( $L, T$ )

GFP and Okoumé panels are constituted of orthotropic layers (veneers) having principal material axes that coincide with the longitudinal ( $L$ ) and transversal ( $T$ ) geometrical directions of the panels (see Fig. 3). On a macroscopic scale, they can be treated as homogeneous orthotropic materials with the  $L$  and  $T$  axes as the principal axes of the equivalent material.

Homogenized elastic material properties, provided by the manufacturers, are reported in Table 1, where the  $L$  and  $T$  subscripts refer to the longitudinal and

transversal directions, respectively. These values will subsequently be used in the finite element simulations.

**Table 1** Mechanical properties of GFP and Okoumé laminated wood

Plywood	Characteristic strength								Mean Modulus of Elasticity		Mean Shear Modulus
	Bending		Compression		Tension		In plane shear		Tension and Compression		In plane shear
	$f_{m,L}$ MPa	$f_{m,T}$ MPa	$f_{c,L}$ MPa	$f_{c,T}$ MPa	$f_{t,L}$ MPa	$f_{t,T}$ MPa	$f_{v,L}$ MPa	$f_{v,T}$ MPa	$E_L$ MPa	$E_T$ MPa	$G_{LT}$ MPa
GFP (3 layers)	15.8	2.6	7.3	4.7	4.8	3.2	1.5	1.5	6667	4333	720
Okoumé (4 layers)	35	32.4	10	28.5	6.1	17.4	7	7	2398	6852	552

For simplicity, the two textile modules will be referred to as large-scale (TM1) specimen and intermediate-scale (TM2) specimen. Besides a large difference in size and material properties, the textile modules are assembled in a different way. For prototype TM1, the ends of the panels are mechanically linked by means of a pinned connection while hardwood wedge connectors that restrain all degree of freedom are employed to build the second prototype TM2. The construction process of the two prototypes is described below.

## 2.2. Construction of the Textile Modules

### 2.3.1. Pin connection

A pinned connection is used for the assembly of textile module TM1. Practically, the two panels are connected to each other at their ends using a system of steel threaded rods with nuts and washers. The starting point for the assembly procedure is illustrated in Fig 4. For convenience, the global reference coordinate system  $(x,y,z)$  is introduced such as the vertical  $z$ -axis crosses panel 1 and panel 2 at

points A1 and A2, respectively. The two points have the same geometrical position taken as the origin A of the global system. Strictly speaking, point A1 belongs to the lower face of panel 1 while point A2 is on the upper face of panel 2, with the same in-plane coordinates  $L=w/2$ ,  $T=0$  in the local frame  $(L,T)$  of the panels (see Fig. 3). The middle surfaces of the panels are positioned parallel to the plane  $(x,y)$  and symmetrically rotated about the  $z$ -axis by an angle  $\alpha = 10^\circ$ . Then, the panels are linked to each other at points A1 and A2 using the steel threaded rod (not represented in Fig. 4), restraining thus their relative displacement at A while keeping the rotation free along the threaded rod axis. Note that the threaded rod axis initially coincides with the  $z$ -axis but will not keep this direction afterwards.

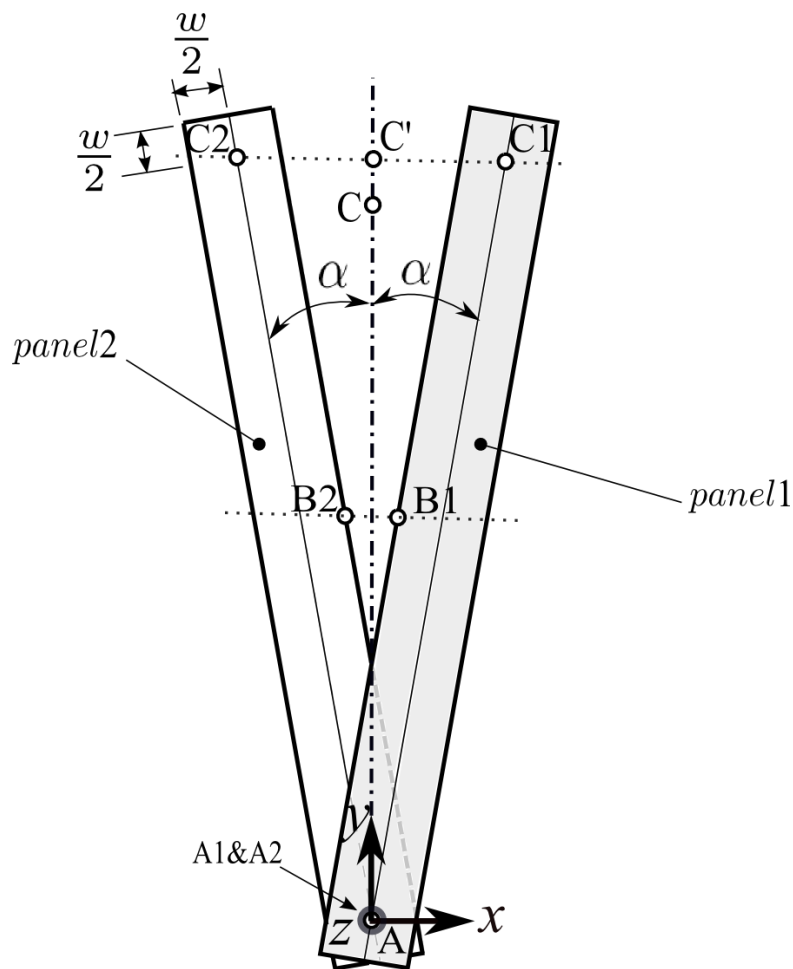


**Fig. 4** Assembly procedure and associated coordinate system

Let now consider the opposite points C1 and C2 (see Fig. 4) having local in-plane coordinates ( $L=l-w/2$ ,  $T=0$ ) such as  $AC_1=AC_2=l-w=11.55\text{m}$ . The line (C1C2) meets perpendicularly the y-axis at point C'. In other words, one has an isosceles triangle (AC1C2) whose base is (C1C2). Practically, the panels are pulled together at points C1 and C2 by means of cables to a third common point C belonging to the y-axis. The distance AC is typically less than AC'. The panels that become doubly curved are again pin-connected at C by means of a second threaded rod. During this operation, the mid-points B1 and B2 of two panel edges come into contact at a point B that corresponds to the maximum height of the resulting structure (Fig. 5). The maximum height (i.e. distance BB') and span (i.e. distance AC) for TM1, are respectively 1.5 m and 10.050 m.

It is worth noting that the two threaded rod axes and point B belong to the vertical plane (y,z). Denoting B' the vertical projection of B onto the y-axis, one has an isosceles triangle ABC of height equal to the line segment BB' and base  $AC=2AB'$ . Moreover, the two threaded rod axes are symmetrically oriented with respect to the axis BB'.

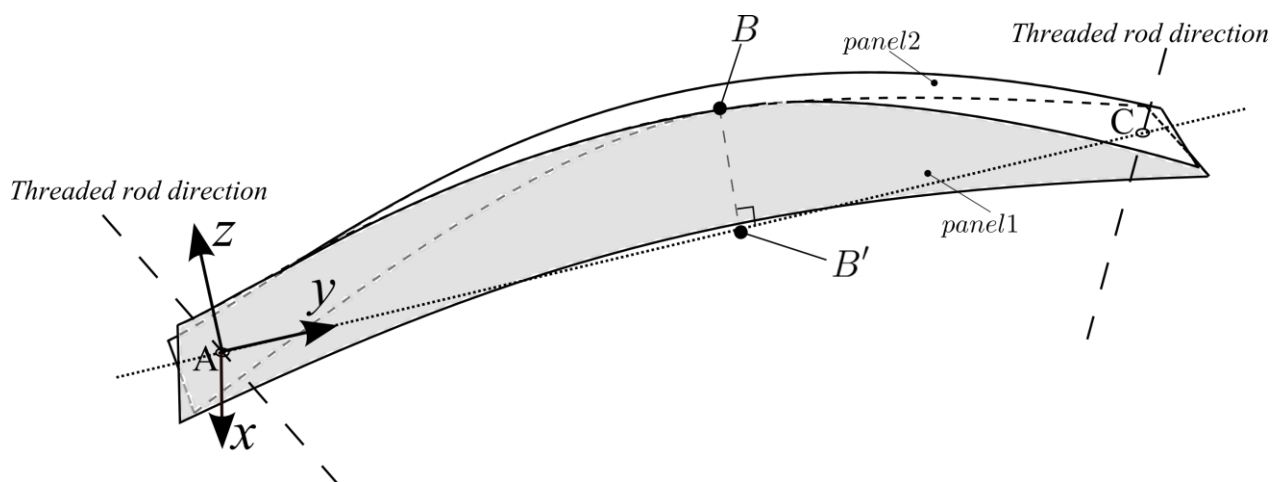


**Fig. 5** Textile module geometry with doubly curved panels

Finally, the two ends of the Textile Module TM1 are firmly fixed on the ground by using a special steel connector (see Fig 6a), restraining thus all displacements and rotations along the corresponding panel edges.

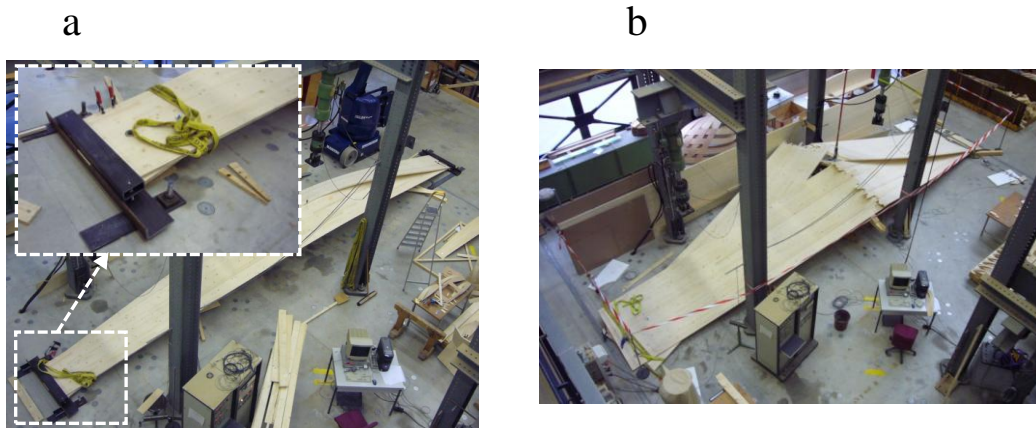


**Fig. 6** (a) Prototype TM1 and steel connector used to fix it on the floor

(b) Failure during the assembly process

Various assembly conditions can readily be imposed on the panels of Textile module, modifying accordingly its final shape and structural behavior. The selection of the type of connectors to be used depends on the assembly conditions under consideration.

Finally, it is noted that the assembly conditions may have a significant influence on the strength of the structure. An early prototype (TM0), constituted of panels with the same characteristics than TM1 except of the width  $w$  equal to 1.650 m, was broken in two after the nuts were tightened in the final step. Both panels failed in two parts at the middle (Fig. 6b) because of the stresses induced.

### **2.3.2. Wedge connection**

A second type of connection, referred simply to as “wedge connection”, is employed for the construction of prototype TM2. As indicated in Fig. 7, two identical sets of three wedge elements are used to connect the panels to each other and fix the whole structure on the ground. The different elements are machined by cutting a block

of hardwood of length 20 cm and cross-sectional area  $w/2 \times w/4 = 12 \times 6 \text{ cm}^2$  along two oblique cutting planes with different orientations (see Fig. 7). The resulting top (*Wedge 3*) and bottom (*Wedge 1*) elements have thus one cross section at right angle and the other obliquely oriented with respect to the lateral faces. Before cutting, three holes of diameter 10 mm have been drilled along the length of the wooden block as indicated in Fig. 7, for the introduction of a tightening system composed of threaded rods and nuts.

Specifically, positioning the structure on the ground is achieved by means of the supporting element *Wedge 1*. The intermediate element (*Wedge 2*) permits the relative position of the panels to be accurately controlled on the constrained areas (assembly conditions). The last wedge element (*Wedge 3*) is practically used to connect the panels together by simply tightening the nuts, aligning thus the three wedges vertically. In particular, this locking device allows the module to be fully clamped on the ground.

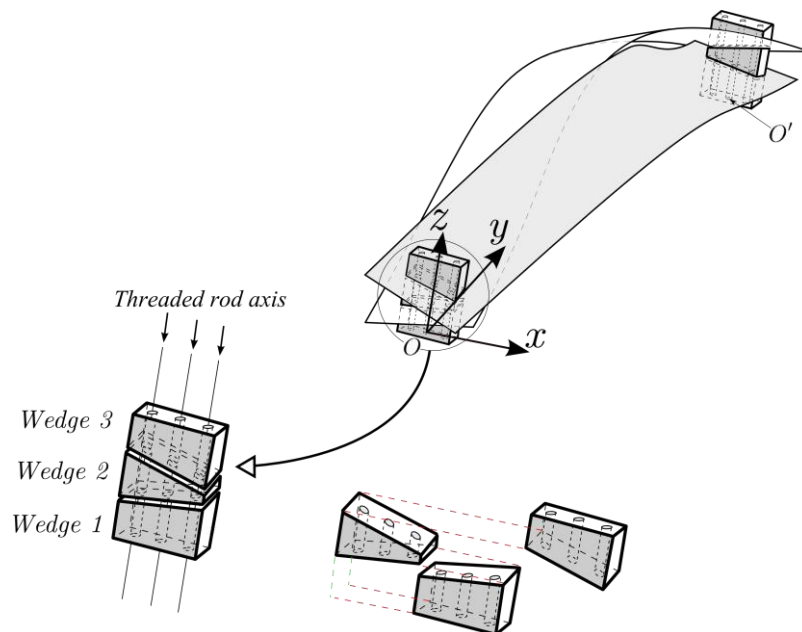


**Fig. 7** Textile module assembled with wedge connection.

The positions of the two oblique (cross-sectional) planes can readily be described by means of six assembly parameters ( $\theta_{x1}, \theta_{x2}, \theta_{y1}, \theta_{y2}, d, d'$ ) as presented in Fig. 8. The origin  $O$  of the reference coordinate system  $(x,y,z)$  is placed at the center of the bottom section of *Wedge 1*. Sketched in Fig. 8 is the final shape of the module where the vertical  $z$ -axis crosses the panel 1 and panel 2 at points  $A1$  and  $A2$  whose respective coordinates are  $(0, 0, d+d')$  and  $(0, 0, d')$ . Unlike prototype TM1, they no longer occupy the same position because of the introduction of *Wedge 2*. It is noted that the threaded rod axes, keeps keep a fixed orientation corresponding to the vertical  $z$ -axis during the assembly. Moreover,  $A1$  and  $A2$  are centroidal points for the contact areas  $p1$  and  $p2$ , whose orientations with respect to the  $x$ -axis and  $y$ -axis are given by the two angles  $\theta_{x1}, \theta_{y1}$  and  $\theta_{x2}, \theta_{y2}$  respectively.

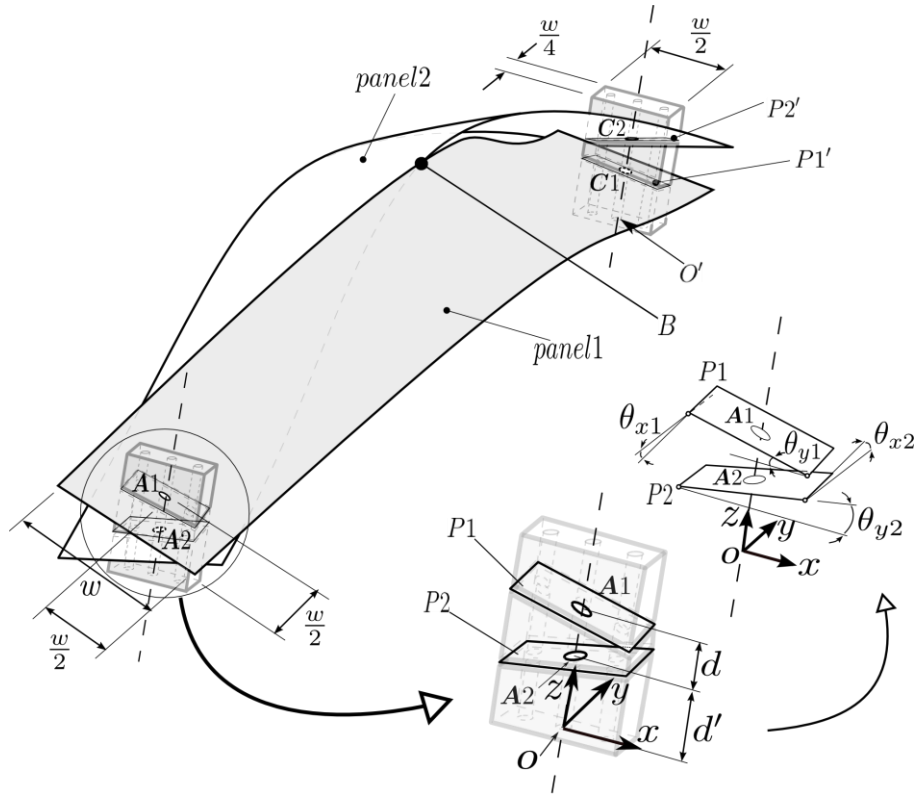


**Fig. 8** Definition of the assembly parameters

Similarly, the opposite points  $C1$  and  $C2$  are centroidal points for the contact areas  $p1'$  and  $p2'$  as defined in Fig. 8. Point  $C1$  is now located under point  $C2$  and

their respective coordinates are given by  $(0, s, d')$  and  $(0, s, d+d')$ . Denoting  $O'$  the intersection of the vertical axis passing through these points and the  $y$ -axis, one has  $s=OO'$ . In this case, the angles  $-\theta_{x1}$  and  $-\theta_{y1}$  (resp. the angles  $-\theta_{x2}$  and  $-\theta_{y2}$ ) orientate the plane  $p2'$  (resp. the plane  $p1'$ ) with respect to the  $x$ -axis and  $y$ -axis.

As for prototype TM1, an isosceles triangle  $OBO'$  can be constructed where vertex  $B$  is defined as the common position of the contacting points  $B1$  and  $B2$ . Again,  $B'$  denotes the vertical projection of the vertex  $B$  on the opposite side  $OO'$ .



**Fig. 9** Textile module TM2 with wooden base

Fig. 9 shows textile module TM2 that is fixed on a thick wooden base using the previous wedge connections. The maximum height  $BB'$  corresponds to 0.360 m, the span  $s$  is equal to 2.305 m and the assembly parameters are chosen to be  $\theta_{x1} = 17^\circ, \theta_{x2} = 11.5^\circ, \theta_{y1} = 14.5^\circ, \theta_{y2} = -8^\circ, d = 76 \text{ mm}, d' = 47.7 \text{ mm}$ .

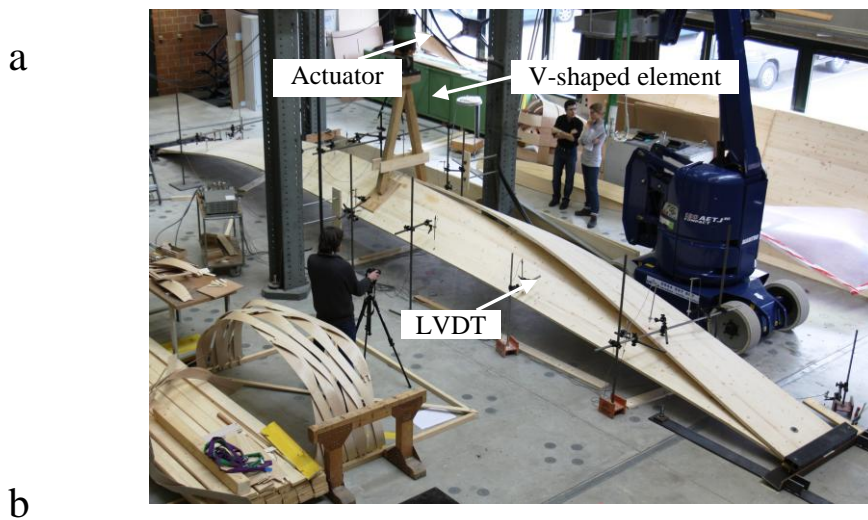
#### **2.4. Test setups and measurement equipment**

The test setup that is used for the experiments is shown in Figs 10 a,b for prototypes TM1 and TM2, respectively.

The ends of prototype TM1 are clamped on the floor by means of the steel connector shown in Fig. 6. A hydraulic actuator from Walter&Bai Company with a

maximum force capacity of  $\pm 500$  kN is used to load the prototype at mid span. An additional V-shaped element (made of hardwood) is attached to the actuator for transferring the load on each panel as indicated in Figs 10a and 11a. During the test, the load is applied up to the ultimate limit state in displacement control with a constant displacement rate of 6 mm/min.

Prototype TM2 and its wooden base are placed on two concrete blocks as shown in Fig. 7. In this case, a hydraulic actuator with a maximum force capacity of  $\pm 300$  kN is used for applying the bending load at the prototype mid span. For an accurate measurement of the force, a load cell of 5KN is added as indicated in the insert of Fig. 10. A specially-designed wooden element with two steel parallel rods is fastened to the actuator for distributing the load on each panel (see Figs 10b and 11b). Again, the test is run in displacement control (constant rate of 3 mm/min) and the prototype loaded up to 0.5 kN.



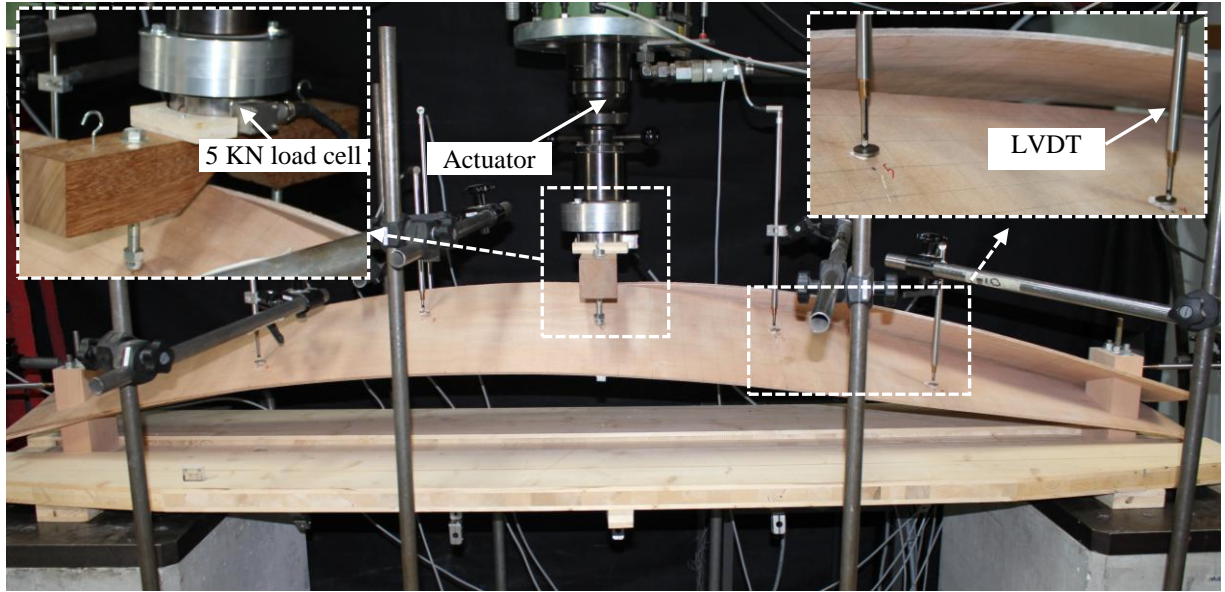


**Fig. 10** Test setup for (a) prototype TM1 (b) prototype TM2

In both cases, the resulting deflections are recorded at several positions along the prototype surface using external transducers mounted on self-supporting vertical steel rods as shown in Figs. 10a and 10b. Specifically, linear variable differential transducers (LVDTs) whose measurement range is  $\pm 100$  mm are employed for measuring the vertical component of the displacement for prototype TM1. Data are typically recorded at three positions that are numbered 1, 2 and 3 in Fig. 11a. The positions of LVDTs in the local frame ( $L, T$ ) are: LVDT1( $L=6.1875$  m,  $T=-0.4125$  m), LVDT2( $L=8.075$  m,  $T=0.4125$  m) and LVDT3( $L=1.25$  m,  $T=0.4125$  m).

For prototype TM2, LVDTs with measurement ranges of  $\pm 30$  mm and  $\pm 50$  mm are placed at seven positions that are indicated in Fig. 11b. Those with measurement ranges of  $\pm 50$  mm are only used to record the vertical displacements at points 4 and 5. For positions 6 and 7, the transducers are directed perpendicular to the top wedge connection in order to check its deformation along the horizontal direction ( $y$ -axis) during loading. As it can be seen in Fig. 10b, small circular pieces of metal are glued on the panels to provide a flat mounting surface in order to maintain the contact with the transducers during the test. A grid mesh constituted of  $78 \times 8$  elements

of  $3 \times 3 \text{ cm}^2$  size, has also been drawn on the upper surface of each panel. This grid corresponds to the numerical mesh used in the finite element analysis. Finally, the positions of LVDTs in the local frame ( $L, T$ ) are given by: LVDT1( $L=0.54 \text{ m}$ ,  $T=0.06 \text{ m}$ ), LVDT2( $L=0.84 \text{ m}$ ,  $T=-0.03 \text{ m}$ ), LVDT3( $L=1.8 \text{ m}$ ,  $T=0.06 \text{ m}$ ), LVDT4( $L=1.5 \text{ m}$ ,  $T=-0.03 \text{ m}$ ) and LVDT5( $L=0.84 \text{ m}$ ,  $T=0.03 \text{ m}$ ).

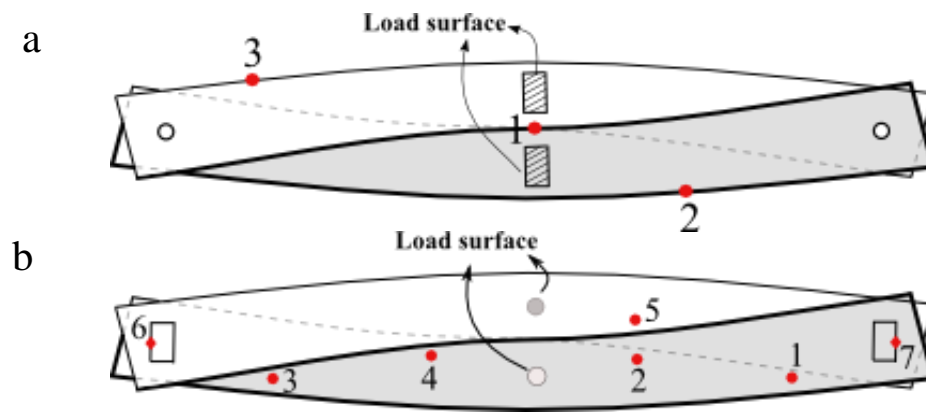


**Fig. 11** Location of measurement points for (a) TM1 (b) TM2 (top view)

### 3. Numerical modeling

A 3D geometrically nonlinear finite element analysis is proposed in this part to simulate the assembly process of the Textile Module, including pinned and wedge connections. It is aimed to calculate the construction stresses (initial stresses) and to reproduce the structural behavior of the structure under bending static loads.

#### 3.1. Material properties

In this study, GFP and Okoumé plywood are modeled as single-layer orthotropic linear elastic materials assuming that the layers are rigidly bonded together. Considering these simplifying assumptions, only four independent engineering constants are required to fully characterize the material behavior, namely : the longitudinal ( $E_L$ ) and transversal ( $E_T$ ) Young's moduli, in-plane shear modulus

( $G_{LT}$ ) and Poisson's ratio ( $\nu_{LT}$ ) [11, 12]. The equivalent unidirectional lamina is consequently assumed to be under a state of plane stress with principal material directions ( $L, T$ ) indicated in Fig. 3. The equivalent material properties are given in Table 1. In the calculation, the average value  $\nu_{LT} = 0.3$  will be considered for the Poisson's ratio. Volumetric changes (shrinkage or swelling of wood panels) due to moisture loss or gain are not taken into account here.

### 3.2. Finite Element model

The commercial FE code ABAQUS is used to build a 3D model of the assembly process for the Textile Module. Because large rotations and deflections as well as boundary nonlinearities (i.e. sudden change in contact conditions between the panels) are expected, a geometrically nonlinear analysis is considered where the specified displacements and loads are applied incrementally.

Each panel is discretized by means of six-node triangular thin shell elements of uniform size (no refinement). Specifically, fully integrated STRI65 elements with five degrees of freedom per node (three displacements  $u_x, u_y, u_z$  and two rotations  $\theta_x, \theta_y$ ) are used. These elements, adapted for large rotation but small strain, provide accurate solutions in the framework of the classical (Kirchhoff) shell theory, where the shell normal remains perpendicular to the shell reference surface (i.e. negligible transverse shear) [13-15].

An implicit time-integration procedure that relies on the Newton-Raphson iterative scheme [16] is typically used to solve the simultaneous incremental nonlinear equations. Accordingly, an estimate of the incremental displacement field satisfying the displacement and traction boundary conditions is obtained at the end of a generic

time increment. In this analysis, the calculations are achieved with a maximum time step of 0.1 for each increment.

### 3.3. Boundary and assembly conditions

The simulation of the Textile Module with pinned and wedge assembly conditions requires considering the construction procedure presented in section 2.2. The same nomenclature is repeated here. Thus, rectangular shell surfaces are used to represent the panels and are positioned in the global coordinate system  $(x,y,z)$  of Abaqus as indicated in section 2.2. In particular, they are symmetrically rotated by an angle  $\alpha$  ( $\alpha=10^\circ$  is taken here) about the global  $z$ -axis. Then, the assembly process is simulated by applying appropriate boundary and assembly conditions on the panels as detailed below for the pinned and wedge connections.

For the pinned connection (prototype TM1), the procedure is as follows:

- The boundary conditions  $u_x = u_y = u_z = 0$  ( $u_i$  is the displacement component in the  $i$ -axis direction) are imposed at points A1 (belonging to panel 1) and A2 (belonging to panel 2). Recall that these points are located at the origin A of the frame.
- At points C1 and C2 (Fig. 4), only the vertical displacement  $u_z = 0$  is imposed. Consequently, these points are constrained to stay in the plane  $(x,y)$
- The displacement vectors  $\mathbf{u}_{C1} = -u_C \hat{\mathbf{e}}_1$  and  $\mathbf{u}_{C2} = u_C \hat{\mathbf{e}}_1$  ( $\hat{\mathbf{e}}_1$  is the unit vector in  $x$  direction) are applied to points C1 and C2 respectively to match them to the common point C' of the  $y$ -axis such as

$$u_C = (l - w) \sin(\alpha) \quad (0)$$

where  $u_C$  is equal to 2005.64 mm and 364.66 mm for TM1 and TM2, respectively.

- The mid-points B1 and B2 of the panel edges are simultaneously shifted to the contact point B, by applying the displacement vectors  $\mathbf{u}_{B1} = -u_B \hat{\mathbf{e}}_1 + w_B \hat{\mathbf{e}}_3$  and  $\mathbf{u}_{B2} = u_B \hat{\mathbf{e}}_1 + w_B \hat{\mathbf{e}}_3$  ( $\hat{\mathbf{e}}_3$  is the unit vector in  $z$  direction) at points B1 and B2 respectively. The expression of  $u_B$  for this transformation can be determined as

$$u_B = (l - w) / 2 \cdot \sin(\alpha) - w / 2 \cdot \cos(\alpha) \quad (001)$$

with respective numerical values of 623.66 m and 64.15 mm for TM1 and TM2.

The design parameter  $w_B$  is imposed, modifying the  $y$ -coordinate of point C' that becomes point C (see Figs. 4 and 5). Note that  $w_B$  corresponds to the distance BB' in Fig. 5.

For the wedge connection (prototype TM2), the procedure becomes:

- The boundary conditions  $u_x = u_y = 0$  are imposed at points A1 and A2
- $u_z = d'$  is imposed at points A2 and C1, while  $u_z = d' + d$  is imposed at points A1 and C2. For the definition of  $d$  and  $d'$  see Fig. 8.
- $\theta_x = \pm\theta_{x1}, \theta_y = \pm\theta_{y1}$  are applied to constrain the nodes on the areas  $p1$  and  $p2'$  and  $\theta_x = \pm\theta_{x2}, \theta_y = \pm\theta_{y2}$  to constrain the areas  $p2$  and  $p1'$ .
- The displacements (in  $x$ -direction) at points C1 and C2 are the same as those obtained for the pin connection (see Eq. 1). As previously, the points are free to move in the  $y$ -direction to the common point C such as  $AC = s$ .
- For the wedge connection, only one displacement component (in  $x$  direction) is needed to position points B1 and B2 to the common point B. So, the displacement vectors  $\mathbf{u}_{B1} = -u_B \hat{\mathbf{e}}_1$  and  $\mathbf{u}_{B2} = u_B \hat{\mathbf{e}}_1$  should be

applied to points B1 and B2 respectively. The expression of  $u_B$  is given by Eq. 2.

### 3.4. Contact interaction

To prevent interpenetration of the two panels, contact regions have to be defined. The general finite-sliding, surface-to-surface algorithm of Abaqus/Standard is used, allowing arbitrary large sliding as well as large rotations and deformations of the surfaces. A frictionless hard contact pressure–overclosure relationship is considered, for which the penetration of the slave surface into the master surface is minimized and no tensile stress is transferred through the interface. Master ( $MS1$ ,  $MS2$ ) and slave ( $SS1$ ,  $SS2$ ) surfaces that can potentially come into contact are specified in Fig. 12 by dividing each panel in two regions. Moreover, surface  $SS1$  (resp.  $SS2$ ) is located on the lower face of *panel1* (resp. *panel 2*) while  $MS1$  (resp.  $MS2$ ) belongs to the upper face of *panel1* (resp. *panel 2*). The two contact surface pairings ( $MS1$ ,  $SS2$ ) and ( $MS2$ ,  $SS1$ ) can then be identified for the tracking contact algorithm.

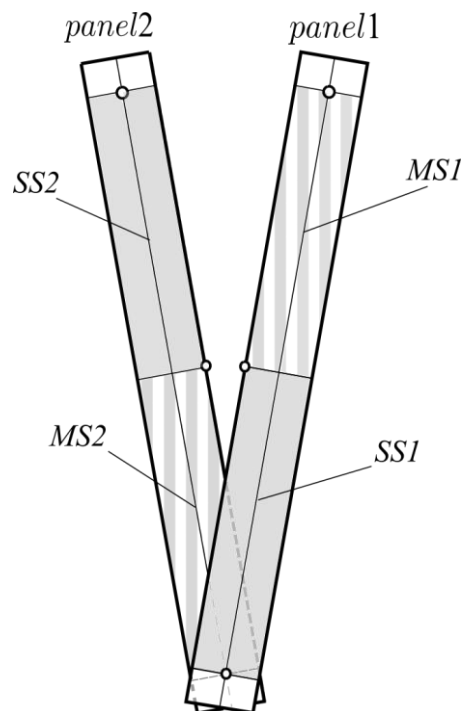


**Fig. 12** Definition of contact interaction between the panels

Frictional effects can be included by considering the (simplest) classical isotropic Coulomb model to describe the frictional behavior between the contacting panels. Representative values of 0.3 and 0.5 will be taken for the (static) coefficient of friction  $\mu$  in our case.

### 3.5. Numerical results

Figure 13a shows the 3D initial shapes obtained numerically for the large-scale and intermediate-scale Textile Modules. The maximum in-plane principal stresses induced during the construction of the Textile Modules are also visualized in Fig. 13b. For the large scale geometry, two widths have been considered for the panels (i.e.  $w=1.650$  m and  $w=0.825$  m), corresponding to the prototypes TM0 and TM1. The FE mesh incorporates STRI65 shell elements, with an element mesh size of 110 mm. Preliminary calculations were conducted with several element mesh sizes ranging from 80 to 150 mm, revealing a difference less than 2% for the in-plane principal stresses. Therefore, in order to reduce the computational time, a uniform mesh size of 110 mm (resp. 20 mm) is chosen for the simulation of large (resp. intermediate) scale geometries. Inspection of Fig. 13b, clearly indicates that maximum initial stresses are located at the contact point B. Table 2 gives the numerical values of the stress components at point B for prototypes TM0, TM1 and TM2.

**Table 2** Construction stresses values at point B for TM0, TM1 and TM2

	TM0	TM1	TM2
$\sigma_{LL}$ (MPa)	45.1	18.01	9.61
$\sigma_{TT}$ (MPa)	-3.3	-0.302	-0.61
$\sigma_{LT}$ (MPa)	0.65	0.248	0.48

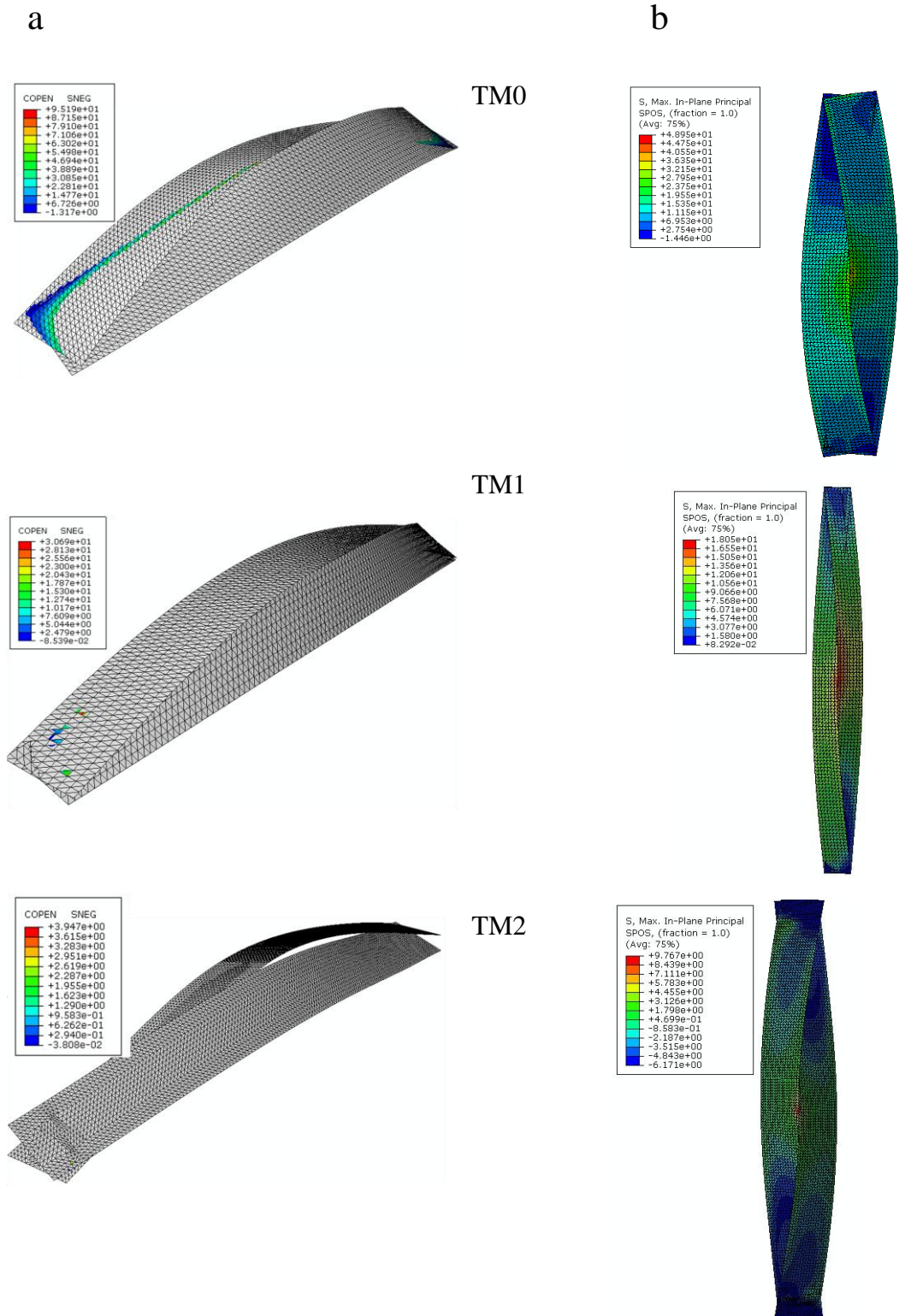


**Fig. 13** (a) Simulated initial shapes and visualization of gaps between contacting surfaces of TM0, TM1 and TM2 (b) Corresponding maximum in-plane principal stresses

The Tsai-Hill failure criterion is now considered to estimate the macroscopic strength of the Textile module. According to the Tsai-Hill failure theory [11] the macromechanical failure criterion for anisotropic materials is given by

$$I_F = \frac{\sigma_{LL}^2}{f_{m,L}^2} - \frac{\sigma_{LL}\sigma_{TT}}{f_{m,L}^2} + \frac{\sigma_{TT}^2}{f_{m,T}^2} + \frac{\sigma_{LT}^2}{f_v^2} \leq 1 \quad (3)$$

where  $\sigma_{LL}$ ,  $\sigma_{TT}$  and  $\sigma_{LT}$  are the local stresses in the orthotropic material directions. In Eq. 3,  $f_{m,L}$ ,  $f_{m,T}$  and  $f_v$  ( $= f_{v,L} = f_{v,T}$ ) are bending and in-plane shear strengths of the laminated wood materials that are given in Table 1. Values of  $I_F$  greater than 1.0 may lead to failure. In Table 3,  $I_F$  is calculated for prototypes TM0, TM1 and TM2 with the values of stresses taken from Table 2. According to the Tsai-Hill criterion (Eq. 3), a module having the same characteristics than prototype TM0 should probably fail during the assembly process as it was experimentally observed in the laboratory.

**Table 3** Maximum value of  $I_F$  for prototypes TM0, TM1 and TM2

	TM0	TM1	TM2
$I_F$	9.3	1.3	0.08

Although this criterion strictly predicts failure for TM1, it should be noted that the value  $f_{m,L} = 15.8 \text{ MPa}$  provided by the company for GFP material is rather conservative. Three-point bending tests, achieved with 26 GFP plates of size  $486 \times 50 \text{ mm}^2$ , revealed that a bending resistance of  $24 \text{ MPa}$  could be reached for 62% of them. Nevertheless, due to the presence of defaults (i.e knots), a relatively large variability in the results was observed with bending strength values ranged from 4.3 to 55 MPa. If one takes  $f_{m,L} = 24 \text{ MPa}$ , Eq. 3 gives 5.1 MPa and 0.63 MPa for TM0 and TM1, respectively.

## 4. Results and Discussion

To compare the experimental and simulated initial shapes for TM2, the  $z$ -coordinates of points 1 to 5 (indicated in Fig. 11b) in the global frame  $(x,y,z)$  are reported in Table 4. It can be seen that a good agreement exists between the values obtained from FE model and those measured with the prototype. The maximum discrepancy is found to be 14% at point 4.

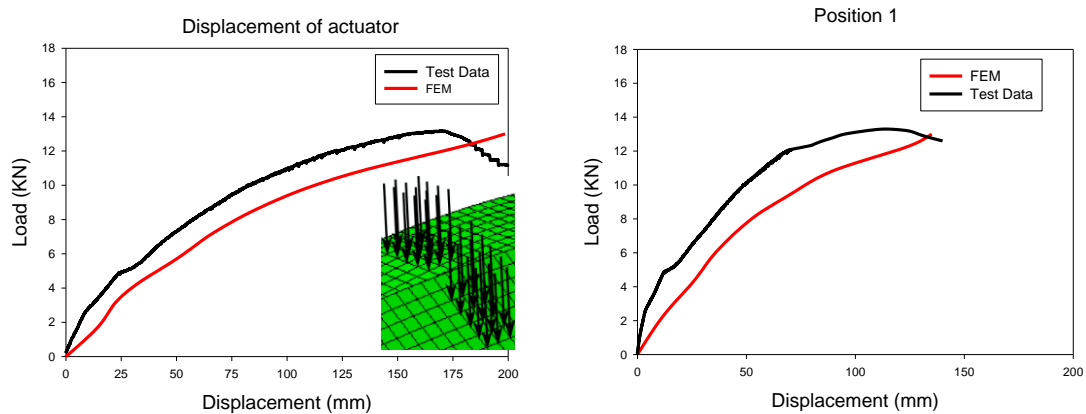
**Table 4**  $z$ -coordinate of points 1 to 5 in global frame  $(x,y,z)$

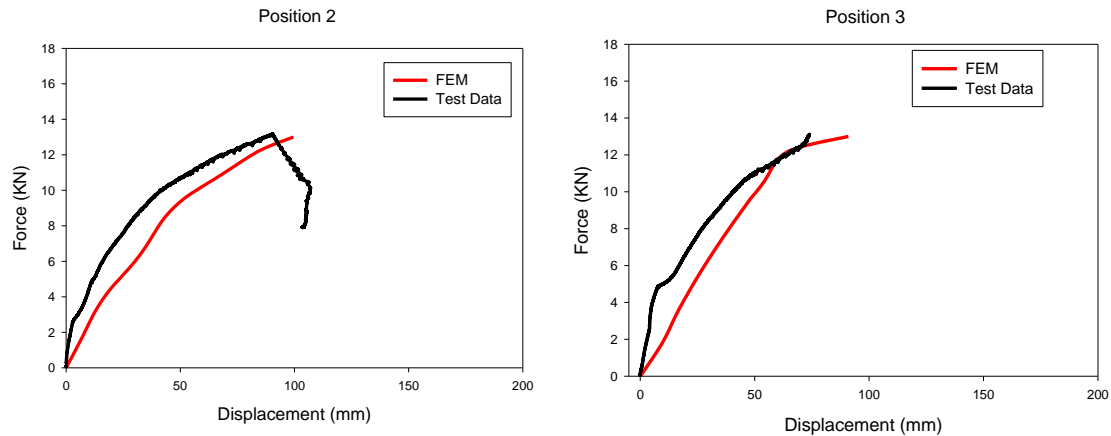
	Point 1	Point 2	Point 3	Point 4	Point 5
Experimental values (mm)	198	271	135	220	221
FE values (mm)	202	293.6	156.4	257	257.5

Force-displacement curves are displayed in Fig. 14 for prototype TM1, where the vertical displacements are recorded at locations (points) 1, 2 and 3 (see Fig. 11a). Compressive loads are given here with positive values. The top left figure provides a plot of the recorded load versus actuator displacement. Experimental results indicate a nonlinear response of the structural element with a maximum sustained load of about 13kN that is reached when the actuator moves down to 170mm. At point1, this maximum load leads to a deflection of 120 mm for the Timber Module (top right figure). Smaller and comparable deflections of about 80mm are obtained at points 2 and 3, farther from the loaded surface. Note that the value at point 1 is much more than the maximum deflection ( $\text{span length}/300=33.5$  mm) of the serviceability limit state, indicating some inherent flexibility of the structure.

Numerically, the module is loaded at midspan such that half of the total (vertical) force is uniformly distributed over a small ( $600 \times 300 \text{ mm}^2$ ) rectangular region of each panel (Fig. 14). In Abaqus, a second “loading” step has been added to the first building step (see section 3.3), allowing the bending load to be applied on the simulated (prestressed) Textile Module. The applied load is linearly ramped over the step up to 13kN. Simulated force-displacement curves are given in Fig 14 at the corresponding experimental positions. The actuator displacement, obtained from the FE model, corresponds to the displacement of a node in the centre of rectangular load area. The graphs indicate a nonlinear (elastic) response of the structure to bending load. The experimental decrease of the load (after 13kN) is clearly not reproduced in the simplified elastic FE model considered.

It is observed that the numerical model tends to underestimate the rigidity of the structure. Differences can be attributed to the material parameters used for the panels. Nevertheless, relatively good agreement is observed between the experimental and numerical predictions.

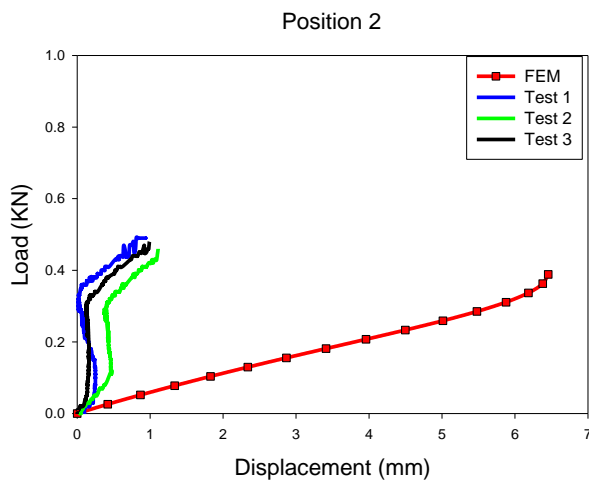
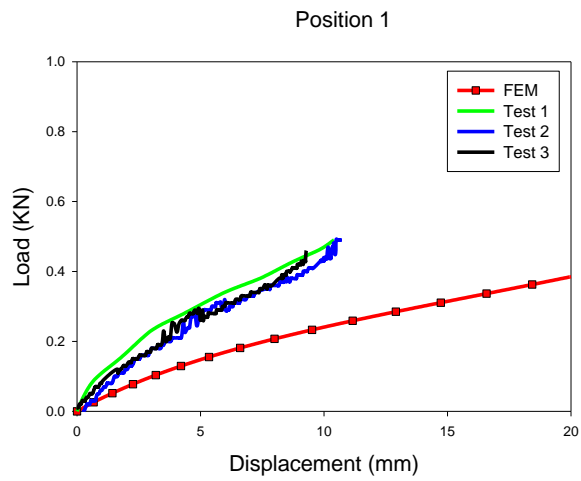
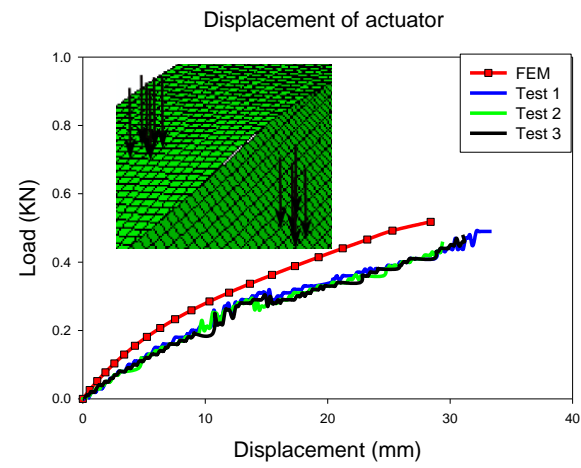




**Fig. 14** Experimental and simulated force-displacement curves (TM1 prototype)

Plotted in Fig 15 are the force-displacement curves obtained for the prototype TM2, when loaded up to 0.5 kN. Compressive loads are again given with positive values. To ensure a good repeatability for the test, the loading procedure is repeated three times and the corresponding curves are referred to as Test1, Test2 and Test3 in Fig 15. The experimental results indicate an overall nonlinear response of the structure. Figures labeled “Position  $i$ ” ( $i=1..5$ ) refer to vertical displacements obtained with transducers positioned at points  $i$  ( $i=1..5$ ) as indicated in Fig. 11b. Interestingly, it appears that certain regions of the structure move up during the test. Thus, all of the considered points shift down (towards the ground) except for point 1 which is shifted in the opposite direction (positive direction of  $z$ -axis). However for simplicity, all the displacements are plotted with positive values in the graphs. At 0.5 kN, a displacement amplitude of 10 mm is measured at point 1 that is comparable to the one recorded at the opposite point 3 (for the same panel). The vertical displacement at point 2 remains surprisingly small (less than 1 mm) compared to the other. A sudden increase of the slope is observed after 0.5mm that cannot be satisfactory explained here and may be due to measurement problems with the LVDT. Next, the slope of the curves suddenly decreases and the recorded data indicate a more expected behavior.

The largest displacements (i.e. about 15mm) are encountered at positions 4 and 5.



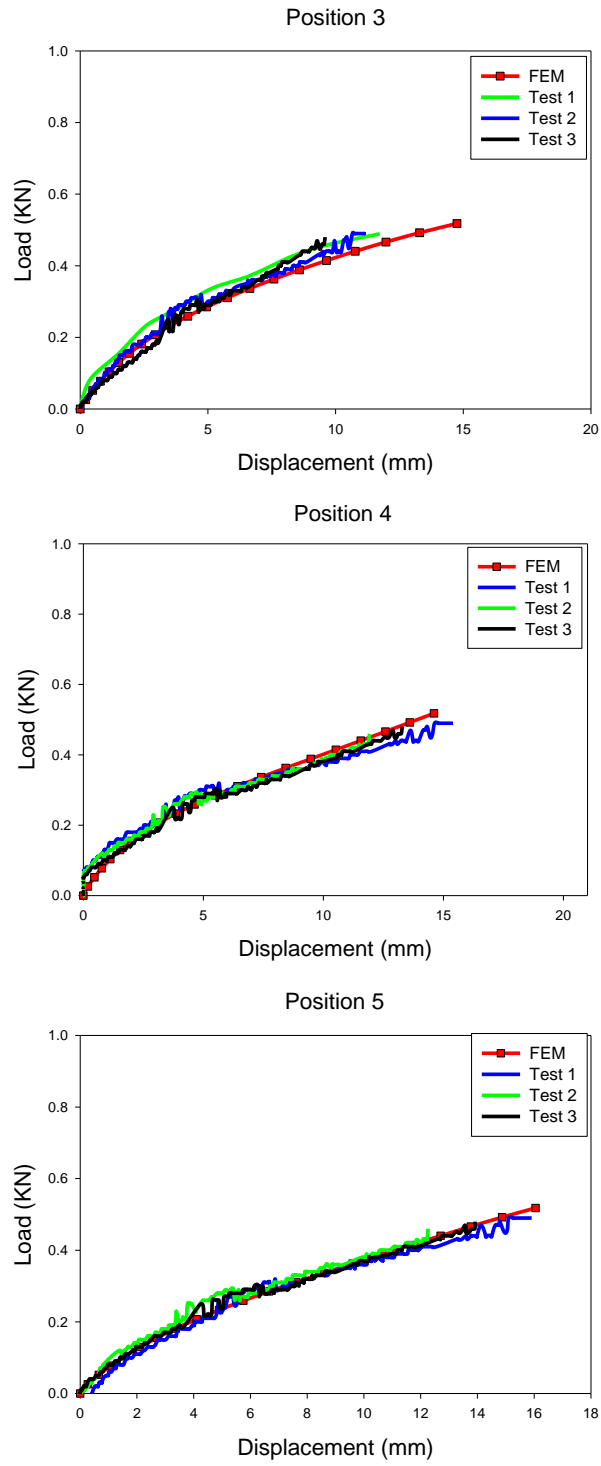


**Fig. 15** Experimental and simulated force-displacement curves (TM2 prototype)

Potential wedge displacements can be recorded with transducers that are positioned horizontally at the two checking positions 6 and 7 (see Fig. 11b). A maximum (horizontal) displacement of 0.2 mm is recorded at these points for the wedges. This indicates a relatively small rotation of the wedge elements due to the bending load. Numerically, the wedges are fixed and the displacement is accordingly zero.

Depicted in Fig. 15 are the load-displacement curves obtained with the FE model. Half of the total (vertical) force is uniformly distributed over a small circular disk of radius 15 mm of each panel (Fig. 15). The applied load is ramped linearly over the step up to 0.5kN. The numerical model correctly reproduces the experimental behavior of the Textile Module at positions 3, 4 and 5. The experimental trend is also satisfactory recovered at position 1. Nevertheless, large discrepancies are observed at position 2 that are attributed to measurement problems, as mentioned previously.

The effects of tangential friction between the contacting panels have also been addressed, taking the values  $\mu=0.3$  and  $\mu=0.5$  for the coefficient of friction. The simulations indicate that these effects do not influence the global behavior of the structure in our case. They are not reported here while the plots are similar to those presented in Fig. 15. It is concluded that no sliding occurs between the surfaces of the panels.

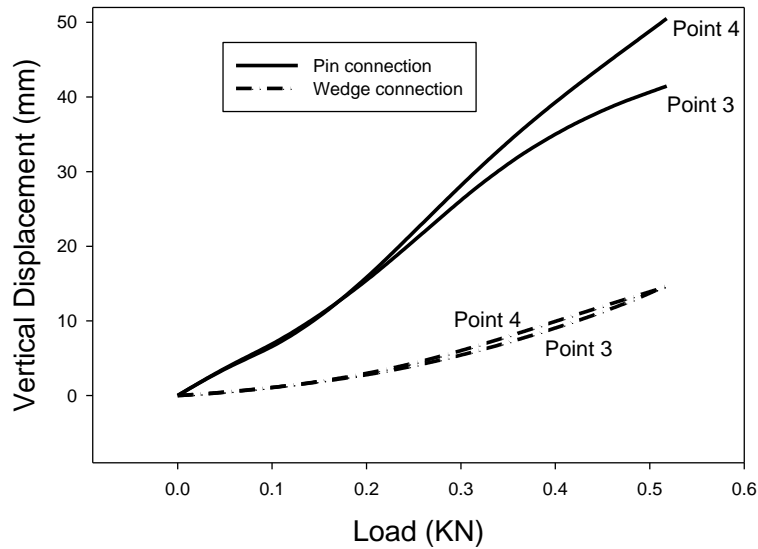


**Fig. 16** Simulated displacements at points 3 and 4 for pin and wedge connections (TM2 geometry)

Finally, the introduction of wedge elements affects significantly the overall rigidity of the structure. Considering again the TM2 geometry, Fig. 16 compares the simulated displacement-load curves obtained at points 3 and 4 when the structure is assembled with pin and wedge connections. In both cases, the same material (i.e. Okoumé plywood) is considered and the modules are loaded up to 0.5 kN. As expected, the wedge connecting elements provide more rigidity for the structure than pin connections.

## 5- Conclusion

In this work, a novel class of timber structures based on the logic and principles of textile techniques has been investigated. A geometrically nonlinear finite element model has been developed for the construction of a single Textile Module including pinned and so-called wedge connections for the assembly conditions. For comparison, large-scale and intermediate-scale experimental prototypes with the previous connections have been constructed.

The proposed analysis aimed first at reproducing the initial shape of the structure and thus evaluating the resulting construction (initial) stresses induced during the

assembly process. It was shown that the simulated shape could satisfactory fit to the experimental one at several measurement points. Moreover, the anisotropic Tsai-Hill criterion based on the maximum induced stresses allows one to select safe design parameters. It was observed that a length-to-width ratio  $l/w=7.5$  for the large-scale GFP panels led to failure during the construction while  $l/w=15$  was safe. For the intermediate prototype ( $l/w=9.75$ ), wedge connections comparatively lead to lower levels of construction stresses and could be adopted at larger scale.

Secondly, the structural behavior of the Textile Module has been examined under bending tests. For the two considered geometries, the resulting deflections have been measured and calculated at several locations. They highlight a nonlinear bending response of the Textile Module. A good agreement is generally observed between the experimental results and the FE predictions at intermediate and large scales. Finally, the introduction of wedge elements was found to improve significantly the overall rigidity of the Textile Module.

## Acknowledgements

The authors would like to thank the Swiss National Science Foundation for supporting this work through contract number 200021-126802. They are also grateful to Mrs. Maria Lindqvist for her participation in the experimental tests.

## References

1. Iffland, J.S.B., *Folded plate structures*. ASCE J Struct Div, 1979. **105**(1): p. 111-123.
2. Happold, E. and W.I. Liddell, *Timber lattice roof for the Mannheim Bundesparkschau*. Structural Engineer, 1975. **53**(3): p. 99-135.
3. Kelly, O.J., et al., *Construction of the downland gridshell*. Structural Engineer, 2001. **79**(17): p. 25-33.
4. Weinand, Y., *Innovative timber constructions*. Journal of the International Association for Shell and Spatial Structures, 2009. **50**(161): p. 111-120.
5. Weinand, Y. and M. Hudert, *Timberfabric: Applying textile principles on a building scale*. Architectural Design, 2010. **80**(4): p. 102-107.
6. D'Amato, E., *Finite element modeling of textile composites*. Composite Structures, 2001. **54**(4): p. 467-475.
7. D'Amato, E., *Nonlinearities in mechanical behavior of textile composites*. Composite Structures, 2005. **71**(1): p. 61-67.

8. Kalidindi, S.R. and E. Franco, *Numerical evaluation of isostrain and weighted-average models for elastic moduli of three-dimensional composites*. Composites Science and Technology, 1997. **57**(3): p. 293-305.
9. Page, J. and J. Wang, *Prediction of shear force using 3D non-linear FEM analyses for a plain weave carbon fabric in a bias extension state*. Finite Elements in Analysis and Design, 2002. **38**(8): p. 755-764.
10. Whitcomb, J., K. Woo, and S. Gundapaneni, *Macro finite element for analysis of textile composites*. Journal of Composite Materials, 1994. **28**(7): p. 607-618.
11. Daniel, I. and O. Ishai, *Engineering mechanics of composite materials*. 1994, Oxford, UK: Oxford University Press.
12. Bodig, J. and B.A. Jayne, *Mechanics of Wood and wood composites*. 1982: Van Nostrand Reinhold Company.
13. *Abaqus: Abaqus Theory Manual Version 6.8-2, RI 02909-2499*. 2009.
14. Ertas, A., J.T. Krafcik, and S. Ekworo-Osire, *Performance of an anisotropic Allman/DKT 3-node thin triangular flat shell element*. Composites Engineering, 1992. **2**(4): p. 269-280.
15. Murthy, S.S. and R.H. Gallagher, *A triangular thin-shell finite element based on discrete Kirchhoff theory*. Computer Methods in Applied Mechanics and Engineering, 1986. **54**(2): p. 197-222.
16. Reddy, J.N., *An introduction to non-linear finite element analysis*. 2004, New York: Oxford University Press.